Boehmite nanorod/gold nanoparticle nanocomposite film for an easy-to-use optical humidity sensor

Priyank Mohan[a], Ryuzo Shinta[b], Jun Fujiwara[c], Hiroaki Takahashi[a], Derrick Mott[a], Yasufumi Matsumura[b], Goro Mizutani[a], Kentaro Iwami[c], Norihiro Umeda[c], and Shinya Maenosono[a,*]

[a] *School of Materials Science, Japan Advanced Institute of Science and Technology (JAIST), 1-1 Asahidai, Nomi, Ishikawa 923-1292, Japan*

[b] *New Business Development & Promotion Department, Nippon Steel Chemical Co., Ltd., 1 Tsukiji, Kisarazu, Chiba 292-0835, Japan*

[c] *Department of Mechanical Systems Engineering, Graduate School of Engineering, Tokyo University of Agriculture and Technology, Koganei, Tokyo 184-8588, Japan*

*Corresponding author: Prof. S. Maenosono
E-mail: shinya@jaist.ac.jp
Tel: +81-761-51-1611
Fax: +81-761-51-1625

Abstract

Nanocomposite films consisting of gold nanoparticles (Au NPs) and boehmite nanorods (NRs) were synthesized *via* simple wet chemical methods. The nanocomposite film exhibited an excellent optical sensing capability of humidity utilizing the refractive-index-dependent localized surface plasmon resonance (LSPR), which directly enables low-cost and easy-to-use remote humidity monitoring. It has been revealed that the superior performance of the Au-NP/boehmite nanocomposite film is owing to porousness, smoothness, and hydrophilicity of the boehmite matrix.

KEYWORDS: Boehmite; Gold nanoparticle; Composite film; Localized surface plasmon resonance; Humidity sensor

1. Introduction

Humidity is one of the most common physical quantities in our daily lives along with temperature, atmospheric pressure, and other ambient conditions. Historically speaking, the relative humidity of the environment has impacted the quality of life in a variety of ways with both low and high humidity levels affecting health, and impacting living conditions or technology, e.g. leading to mold growth or fouling of surfaces. Recently, the importance of accurate humidity measurement has rapidly grown in diverse areas such as air conditioning for human comfort, combating bacterial growth to industrial process control, and geotechnical measurements. The requirements for humidity monitoring may vary depending on the application and hence various techniques have been employed to perform humidity measurements [1]. For this reason, many different types of humidity sensors have been developed.

One of the oldest sensors in use is the mechanical hygrometer. Although the mechanical hygrometer is inexpensive and easy to implement, its response is generally quite slow, and thus, unsuitable for most of those applications where environmental conditions change rapidly. As another conventional humidity sensor, the chilled mirror hygrometer has been known as the most accurate and reliable humidity sensor and is widely used for the determination of the dew point. However, this method is relatively expensive and requires regular maintenance due to its susceptibility to surface contamination. Among other conventional humidity sensors, the infrared (IR) absorption hygrometer, electronic humidity sensors (capacitive- and resistive-based) and optical waveguide sensors are commonly used depending on the purpose.

The above-mentioned conventional humidity sensors, however, are generally not suitable for

humidity measurement near flammable liquids, in explosive atmosphere or in situations where *in-situ* and remote monitoring are required. Fiber-optics based humidity sensors have some unique features including small size, multiplexing and remote sensing capabilities, and thus, have attracted attention over the years even though there are still some problems to be solved such as the limitations of the operating range and accuracy. Typically, fiber-optics based humidity sensors involve direct spectroscopic (absorption- and fluorescence-based), evanescent wave (absorption-, refractive-index-, and scattering-based), in-fiber grating, and interferometric methods [1]. Each fiber-optics humidity sensor has had their own particular advantages and disadvantages in terms of cost, accuracy, operating range, ease of use, background interference, etc. For this reason, it is required to develop a new fiber-optics based humidity sensor that is accurate, easy to use, robust, can be employed in a wide range of environments and is low cost.

Noble metal nanoparticles (NPs) have intriguing optical properties that make them ideal candidates for use as probes in chemical/biological sensing applications [2-7]. By utilizing the intriguing optical properties of metal NPs including localized surface plasmon resonance (LSPR), it becomes possible to detect minute amounts of chemical/biological substances [8-10]. Specifically, the LSPR peak wavelength of gold (Au) NPs strongly depends on the local environment, e.g. the refractive index of the surrounding medium and the interparticle distance, and thus, one can spectroscopically detect an analyte using the LSPR peak shift.

Recently, on the other hand, Au NP-containing metal oxide nanocomposite films have been utilized for gas sensing applications [11-15]. Among those Au NP/oxide composite gas sensors, porous

semiconductor metal oxides such as SnO_2, ZnO, TiO_2, and NiO have been widely used as a sensing/supporting material. In most cases, the gas detection relies mainly on the electrical resistivity change of the composite film upon adsorption/desorption of gas molecules on the surfaces of the composite film just like the conventional semiconductor gas sensors. Au NPs were typically used as sensitizers and catalysts to enhance the sensitivity and selectivity of these semiconductor metal oxide gas sensors.

By taking advantage of both the refractive-index-dependent LSPR peak of Au NPs and the metal oxide material, it is possible to develop an optical humidity sensor using the Au NP/oxide composite film as a sensing element which can be readily implemented in a fiber-optics system, enabling low-cost and easy-to-use remote monitoring with reasonable accuracy and response time. To achieve this purpose, it is necessary to fabricate a thick porous composite film with a smooth surface to achieve high signal-to-noise ratio and fast response by having a high number density of Au NPs per unit area, high specific surface area and minimization of undesirable geometric scattering at the surface.

Boehmite (γ-AlOOH) has been historically used as catalyst support, filler, abrasive, and electrical insulating materials. Also γ-AlOOH is commonly used as a pigment in ink-jet paper coatings that limit diffusion of the ink away from the point of contact because of its transparency, amenability to calendering, and well-defined porosity [16]. In this study, we used γ-AlOOH as a metal oxide supporting material to fabricate thick, porous, and transparent Au NP-containing metal oxide nanocomposite films for their utilization as LSPR-based humidity and/or gas sensing materials.

In the present study, Au NP-loaded γ-AlOOH nanocomposite films were fabricated *via* wet chemical

methods. The nanocomposite film exhibited an excellent optical sensing capability of humidity utilizing the refractive-index-dependent LSPR, which directly enables low-cost and easy-to-use remote humidity monitoring.

2. Experimental Section

2.1. Materials

Trisodium citrate (purity 99.0 %), hydrogen tetrachloroaurate(III) trihydrate ($HAuCl_4 \cdot 3H_2O$, purity 99.9 %), acetic acid (purity 99.0 %), aluminum acetate, basic [$Al(OH)(OAc)_2$], and common solvents were purchased from Sigma-Aldrich Corp. Hydrogen tetrachloroaurate(III) tetrahydrate ($HAuCl_4 \cdot 4H_2O$, purity >99.0%) was purchased from Kanto Chemical. Water was purified with a Millipore Direct-Q system (18.2 MΩ).

2.2. Syntheses of Au NPs and γ-AlOOH NRs

Citrate-passivated Au NPs of different sizes were synthesized by the Frens method [17]. Briefly, an aqueous solution of $HAuCl_4 \cdot 3H_2O$ (50 mL, 0.25 mM) was vigorously stirred and heated at reflux. Then, an aqueous solution of trisodium citrate (1.25 mL, 1 wt%) was added to the reaction solution. After the addition of the citrate solution, the reaction temperature was kept at 100 ºC for 1 hour. By varying the amount of citrate solution added, monodispersed Au NPs of six different sizes (13.5–78.9 nm) were synthesized.

γ-AlOOH NRs were synthesized by our own method [18]. In a typical synthesis of γ-AlOOH NRs, 3.5 mmol of $Al(OH)(OAc)_2$ was dissolved in 70 mL of distilled water, and then the resulting solution was transferred to an autoclave. The hydrothermal reaction was performed at 180 ºC for 12 hours. After

which the autoclave was cooled down to room temperature, the reaction mixture was taken out, centrifuged and repeatedly washed several times with distilled water. The as-prepared product was dried in an oven at 60 ºC overnight to give white powders of γ-AlOOH NRs.

2.3. Preparation of AuNPs/γ-AlOOH nanocomposite films

2.3.1. In-situ reduction method

γ-AlOOH NRs (6.0 g) were dispersed in a mixture of pure water (17 g) and acetic acid (0.5 g), and then, sonicated for 5 min at room temperature. Subsequently, $HAuCl_4 \cdot 4H_2O$ (1.25 g) dissolved in 17 g of ethanol was added to the dispersion and sonicated for 5 min at room temperature. Then, the dispersion containing γ-AlOOH NRs and Au ions was spin-coated onto a non-alkali glass substrate followed by heat treatment at 70 ºC for 3 min, at 130 ºC for 10 min, and at 280 ºC for 10 min to obtain a AuNPs/γ-AlOOH nanocomposite film with a thickness of about 2 μm.

2.3.2. Direct mixing method

γ-AlOOH NRs (50 mg) were dispersed in a mixture of pure water (350 μL) and acetic acid (20 μL), and then, sonicated for 5 min at room temperature. Subsequently 5 mL of citrate-capped Au NP dispersion was added to the boehmite dispersion dropwise under stirring, and then, the mixed sample was continuously stirred for 45 min at room temperature. After stirring, a thick viscous dispersion was obtained. Finally, the mixed composite was spin-coated onto a pre-cleaned glass substrate followed by heat treatment at 150 ºC for 1 hour (rate of temperature increase was 3 ºC/min) to obtain a AuNPs/γ-AlOOH nanocomposite film with a thickness of about 2 μm.

2.4. Instrumentation and measurements

The samples were characterized by X-ray diffraction (XRD), transmission electron microscopy (TEM), field-emission scanning electron microscopy (SEM), and UV-visible spectroscopy (UV-Vis). XRD data were obtained using a Rigaku SmartLab diffractometer with Cu Kα radiation (λ = 1.54056 Å; 30 kV, 40 mA). TEM images were obtained using an Hitachi H-7100 transmission electron microscope operated at 100 kV. SEM images were obtained using an Hitachi S-4700 field emission scanning electron microscope. UV-Vis spectra were recorded on a Perkin Elmer Lambda 35 spectrometer.

For gas sensing experiments, two different home-made equipments were prepared. One of them was specially designed for humidity sensing experiments as shown in Fig. 1. The purpose of the experiments is to demonstrate how the AuNPs/γ-AlOOH nanocomposite film works as an excellent humidity sensor. The equipment for the humidity sensing experiments consists of two parts: one is a divided flow humidity generator and the other is a temperature-controlled measuring chamber (Fig. 1). The divided humidity generator produces the moist air of a given water vapor concentration by adjusting the proportions of dry and humid air. The humidity of the moist air was monitored in-line using a chilled mirror hygrometer (Shinyei Technology, DewStar S-2S). The measuring chamber was connected to the outlet of the humidity generator and the moist air was introduced into the chamber at a constant flow rate (0.5 L/min). The AuNPs/γ-AlOOH nanocomposite film on a glass substrate whose underside was coated with silver was placed onto a Peltier cooler in the measuring chamber. The temperature at the sample surface was kept constant at 26 ºC. Reflectance measurements perpendicular to the surface of the composite film were performed using a white light source (LS-1 tungsten halogen lamp, Ocean Optics) and a portable fiber-optic spectrometer (Model QE 65000, Ocean Optics). The temperature and humidity

in the chamber were also monitored using a thermo-hygrometer (Model HN-K, Chino).

The second apparatus was specifically designed for experiments focusing on transient response of the nanocomposite film upon adsorption/desorption of gas molecules as shown in Fig. 2. For this purpose, hexane gas was turned into an object of detection, because it is volatile and does little harm to the chamber windows made of polymethyl methacrylate. N_2 gas (99.99%) was used as reference and diluent gas for hexane vapor. Hexane vapor was generated by bubbling N_2 gas through a liquid hexane in a sealed flask (Fig. 2a). The N_2 gas flow rate was kept constant at 150 mL/min by a calibrated mass-flow controller, and then, N_2 or hexane-containing N_2 gas was introduced in the chamber (Fig. 2b). The total volume of the chamber and the tubes is ca. 80 mL, and thus, the delay time at the time of gas switching is virtually negligible. An optical filter and a monochromator were placed in front of the Xe lamp to obtain monochromatic light. The monochromatic beam was modulated by a chopper to obtain 1000 Hz square pulses and was split into two by a quartz plate. One of the beams was detected as a reference signal. The other was loosely focused by a lens on the sample surface in the chamber. The transmitted light was detected by a photo diode and a lock-in amplifier. The lock-in amplifier was synchronized with the 1000 Hz chopper to eliminate noise associated with all of the non 1000 Hz frequencies, which improves the S/N ratio. All experiments were performed at 22±1 ºC.

3. Results and discussion

3.1. Characterization of Au NPs and γ-AlOOH NRs

Mean diameters and size distributions of Au NPs of different sizes are 13.5±0.9 nm, 24.1±1.5 nm, 35.0±3.8 nm, 48.5±4.8 nm, 55.9±4.6 nm, 67.1±6.4, and 78.9±5.6 nm. All samples are relatively

monodispersed with a size distribution of less than 10%. Fig. 3a, b, c and d show TEM images of Au NPs of mean diameter, *D*, of 13.5 nm, 24.1 nm, 48.5 nm, and 78.9 nm, respectively. Fig. 3e shows a TEM image of γ-AlOOH NRs. As seen in Fig. 3e, the NRs have a diameter of about ~10-30 nm and a length of about ~60-400 nm. The γ-AlOOH NRs are readily dispersed in water or other polar solvents at high concentration with excellent colloidal stability. The inset of Fig. 3e shows the XRD pattern of γ-AlOOH NRs indicating that the NRs have an orthorhombic γ-AlOOH single phase. Fig. 4 shows normalized UV-Vis spectra of aqueous dispersions of Au NPs with different sizes. It is clearly seen that the LSPR band is red-shifted and broadened with increasing the Au NP size. The inset of Fig. 4 shows the LSPR peak wavelengths plotted versus *D* having some deviations from the possible linear approximation. Those variations are presumably due to the size distribution of Au NPs.

3.2. AuNPs/γ-AlOOH film prepared by the in-situ reduction method

Fig. 5a, b, c and d show visual appearance, UV-vis spectra, SEM image of the surface and cross-sectional TEM image of AuNPs/γ-AlOOH composite film fabricated *via* the *in-situ* reduction method. The composite film is transparent and reddish-pink in color in ambient conditions (Fig. 5a, top). However, it turns bluish-purple in color when exposed to water (Fig. 5a, bottom) due to an increase in the refractive index of the surroundings (air = 1.000, water = 1.333). The color change is also evidenced by UV-Vis spectra (Fig. 5b). One important aspect of the composite film is the smoothness of its surface which is responsible for transparency (Fig. 5a). As seen in Fig. 5c, the composite film is highly porous even though its surface is rather smooth. Au NPs generated in the porous γ-AlOOH framework are well-separated and uniformly distributed over the entire film as shown in Fig. 5d. However, one of the

common problems of the *in-situ* reduction method is that the size distribution of NPs becomes quite broad. In fact, the Au NPs in the composite film are polydispersed (Fig. 5d).

3.3. Sensitivity factor

It is well-known that the LSPR peak shifts toward longer wavelength with increase in the refractive index of the surrounding medium, the mechanism of which has been elucidated by Mie theory [19]. Typically, in the case of Au NPs, the LSPR peak wavelength (λ_{max}) linearly increases with increasing the refractive index of the surrounding medium (n). The slope of a plot of λ_{max} vs refractive index is the so-called sensitivity factor, $S = d\lambda_{max}/dn$, which is generally used as a measure of sensitivity of LSPR-based sensors [19]. Fig. 6a shows the LSPR peak wavelength as a function of refractive index for AuNPs/γ-AlOOH composite films containing Au NPs of different D fabricated *via* the direct mixing method. Note that all samples are structurally almost the same except for the mean size of Au NPs (data not shown). The UV-Vis spectra were obtained for the AuNPs/γ-AlOOH composite film immersed in methanol, hexane, chloroform and toluene, whose refractive indices are 1.3284, 1.3749, 1.4458 and 1.4969, respectively. In all samples, linear dependence of λ_{max} on n is clearly observed and the S value increases with D as shown in Fig. 6b. According to the discrete dipole approximation (DDA) calculation, S linearly increases with D in the case of spherical Au NPs [19], while S exponentially increases with D in the present study as shown in Fig. 6b indicating that the larger NPs exhibit a higher LSPR peak shift. A value of S of 38±5 nm per refractive index units (RIU) was obtained for D = 13.5 nm, and S systematically increased with D (S = 42±4, 42±5, 47±6, 56±6, 70±4, and 100±8 nm/RIU for D = 24.1, 35.0, 48.5, 55.9, 67.1, and 78.9 nm, respectively). However, increase in D usually induces undesirable

line broadening of the LSPR peak (Fig. 4) which limits the resolution power and whether the spectral change can be distinguished.

3.4. Humidity sensing

To demonstrate how the AuNPs/γ-AlOOH nanocomposite film works as an excellent humidity sensor, we performed humidity sensing experiments using the AuNPs/γ-AlOOH composite film fabricated *via* the *in-situ* reduction method. Fig. 7 shows the evolution of the change in absorbance at 570 nm (ΔA_{570}) for different humidity levels. Fig. 7a depicts a calibration plot of ΔA_{570} as a function of water vapor concentration (V) with a good sigmoidal fit (R^2 = 0.987) within the range of 100 to 35,000 ppm_v (approximately corresponding to the dew point range of −41.2 ºC to 23.3 ºC). The sigmoidal fit is typically used for calibrating the absorbance change as a function of chemical species concentration in different types of absorption-based LSPR sensors [20,21]. The sensor shows reproducible sensitivity for a sequence of measurements. Fig. 7b shows the time evolutions of the water vapor concentration, V, measured by the AuNPs/γ-AlOOH composite film (red curve) and a chilled mirror hygrometer (black curve) for different humidity levels of moist air. Importantly, the response time of the AuNPs/γ-AlOOH composite film was found to be quite fast (ca. <20 sec) and the signal was quickly stabilized.

Because the sensor response is nonlinear in nature as seen in Fig. 7a, development of an adequate calibration methodology is required to expand the range of detection [22]. Moreover, at the time of initial introduction of water-containing air, the overshoot phenomenon is observed. This overshoot phenomenon would be a result of the competition between diffusion and reaction for the gas molecules [23]. Although some problems remain to be solved as mentioned above, it has been clearly demonstrated that the

AuNPs/γ-AlOOH composite film has great potential as a high-performance humidity sensing element which is easily implementable in a conventional fiber-optics system with high accuracy equivalent to a chilled mirror hygrometer in a low-humidity environment.

3.5. Transient response upon adsorption/desorption of hexane

As mentioned above, the AuNPs/γ-AlOOH composite film exhibited a fast response to water vapor. It is possible that the hydrophilic nature of the γ-AlOOH surfaces is a key for the response speed even more than the porous structure of the composite film. To test the hypothesis, we carried out the hexane vapor sensing experiments using AuNPs/γ-AlOOH composite films containing Au NPs with different *D* fabricated *via* the direct mixing method, because hexane is representative of nonpolar solvents which has weak affinity for the hydrophilic surfaces. The analysis of sensing performances revealed an appreciable reproducibility even upon repeated cycling. Fig. 8 shows the isothermal dynamic responses for AuNPs/γ-AlOOH composite films with different *D* (*D* = 13.5, 48.5 and 78.9 nm) to square concentration pulses of hexane at room temperature. The measured transmission dropped off at fixed wavelength (520, 540 and 580 nm for *D* = 13.5, 48.5 and 78.9 nm, respectively) in the presence of hexane vapor due to an increase in the LSPR intensity which is typically observed along with the red-shift of the LSPR peak shift as the refractive index of the surrounding medium increased [24] (see Fig. 5b). When hexane-containing N_2 gas was introduced in the chamber, the adsorption of hexane molecules in pores of the AuNPs/γ-AlOOH composite film takes place, and thus, the refractive index of the local environment of the Au NPs increases resulting to the transmission drop. On the contrary, when N_2 gas was introduced in the chamber, hexane molecules desorbed from the surfaces of the composite film and the transmission

promptly recovers. Time constants of the adsorption and desorption processes were calculated by a single exponential curve fit and found to be 3.4±0.4 min and 0.5±0.1 min, respectively, regardless of *D*. Because the time constant for gas switching is roughly 0.5 min, desorption of hexane would be rather fast. On the other hand, the adsorption rate of hexane is much slower than the desorption rate. This might be due to the hydrophilic nature of the γ-AlOOH surface and the resulting weak interaction between hexane molecules and the γ-AlOOH surface. In the case of water vapor, as discussed above, the response time was found to be very fast (ca. <20 sec), possibly due to a strong interaction between water and the γ-AlOOH surface [25]. Interestingly, the amount of transmission change (ΔT_{max}) for the composite film containing the smallest Au NPs (D = 13.5 nm) is largest (28%). ΔT_{max} is defined as $\Delta T_{max} = 100\times(T_N - T_H)/T_N$ where T_N and T_H are the steady-state transmissions in N_2 and hexane-containing N_2 atmosphere, respectively. For other composite films with D = 48.5 and 78.9 nm, ΔT_{max} are 16.6% and 15.0%, respectively. This trend is completely opposite to the trend observed in the sensitivity factor, *S*, suggesting that the broadening of the LSPR peak exerts an enormous amount of negative influence on the actual sensitivity when the amount of refractive index change is relatively small. This means that one needs to carefully choose an appropriate size of Au NP depending on the application.

4. Conclusion

Au NP-loaded γ-AlOOH nanocomposite films were synthesized *via in-situ* reduction and direct mixing methods. In both cases, we could obtain uniform and clear composite films. The *in-situ* reduction method is more facile than the direct mixing method to form the composite film, while the resulting Au NPs become polydisperse. On the other hand, the direct mixing method gives more uniform films in

terms of Au NP size even though the construction technique is more rigorous than the *in-situ* reduction method. It is worth noting that there is no difference *per se* between the composite films fabricated *via in-situ* reduction and direct mixing methods in terms of the sensing characteristics. By using both methods as the situation demands, we obtained four important findings: first, the sensitivity factor, *S*, exponentially increases with the Au NP size, *D*, unlike the theoretical calculation which predicted the linear dependence of *S* on *D*; second, the AuNPs/γ-AlOOH composite film acts as an excellent LSPR-based humidity sensing element which can be readily implemented in a fiber-optics system and enables low-cost and easy-to-use remote monitoring with reasonable accuracy and response time; third, the AuNPs/γ-AlOOH composite film exhibited a relatively fast response to water vapor due to the hydrophilic nature of the γ-AlOOH surfaces; fourth, the dynamic range is not always large just because *S* is large, and thus, it is important to design optimal size, size distribution and number density of Au NPs depending on the operating conditions.

References

[1] T.L. Yeo, T. Sun, K.T.V. Grattan, Fibre-optic sensor technologies for humidity and moisture measurement, Sens. Actuators A 144 (2008) 280-295.

[2] K.J. Lee, P.D. Nallathamby, L.M. Browning, C.J. Osgood, X.H.N. Xu, In vivo imaging of transport and biocompatibility of single silver nanoparticles in early development of zebrafish embryos, ACS Nano 1 (2007) 133-143.

[3] S.E. Skrabalak, J. Chen, L. Au, X. Lu, X. Li, Y. Xia, Gold nanocages for biomedical applications, Adv. Mater. 19 (2007) 3177-3184.

[4] J. Matsui, K. Akamatsu, N. Hara, D. Miyoshi, H. Nawafune, K. Tamaki, N. Sugimoto, SPR sensor chip for detection of small molecules using molecularly imprinted polymer with embedded gold nanoparticles, Anal. Chem. 77 (2005) 4282-4285.

[5] N.T.B. Thuy, R. Yokogawa, Y. Yoshimura, K. Fujimoto, M. Koyano, S. Maenosono, Surface-enhanced Raman spectroscopy for facile DNA detection using gold nanoparticle aggregates formed via photoligation, Analyst 135 (2010) 595-602.

[6] P. Singh, N.T.B. Thuy, Y. Aoki, D. Mott, S. Maenosono, Intensification of surface enhanced Raman scattering of thiol-containing molecules using Ag@Au core@shell nanoparticles, J. Appl. Phys. 109 (2011) 094301.

[7] D.T.N. Anh, P. Singh, C. Shankar, D. Mott, S. Maenosono, Charge-transfer-induced suppression of galvanic replacement and synthesis of (Au@Ag)@Au double shell nanoparticles for highly uniform, robust and sensitive bioprobes, Appl. Phys. Lett. 99 (2011) 073107.

[8] C. Wang, L. Ma, M. Hossain, H. Wang, S. Zou, J.J. Hickman, M. Su, Direct visualization of molecular scale chemical adsorptions on solids using plasmonic nanoparticle arrays, Sens. Actuators B 150 (2010) 667-672.

[9] W.P. Hall, S.N. Ngatia, R.P. Van Duyne, LSPR biosensor signal enhancement using nanoparticle-antibody conjugates, J. Phys. Chem. C 115 (2011) 1410-1414.

[10] M.K. Fan, G.F.S. Andrade, A.G. Brolo, A review on the fabrication of substrates for surface enhanced Raman spectroscopy and their applications in analytical chemistry, Anal. Chim. Acta 693 (2011) 7-25.

[11] D. Buso, J. Pacifico, A. Martucci, P. Mulvaney, Gold-nanoparticle-doped TiO_2 semiconductor thin films: optical characterization, Adv. Funct. Mater. 17 (2007) 347-354.

[12] D. Buso, M. Post, C. Cantalini, P. Mulvaney, A. Martucci, Gold nanoparticle-doped TiO_2 semiconductor thin films: gas sensing properties, Adv. Funct. Mater. 18 (2008) 3843-3849.

[13] E.D. Gaspera, D. Buso, A. Martucci, Gold nanoparticles to boost the gas sensing performance of porous sol-gel thin films, J. Sol-Gel. Sci. Technol. 60 (2011) 366-377.

[14] D. Barreca, G. Carraro, E. Comini, A. Gasparotto, C. Maccato, C. Sada, G. Sberveglieri, E. Tondello, Novel synthesis and gas sensing performances of CuO-TiO_2 nanocomposites functionalized with Au nanoparticles, J. Phys. Chem. C 115 (2011) 10510-10517.

[15] E.D. Gaspera, M. Karg, J. Baldauf, J. Jasieniak, G. Maggioni, A. Martucci, Au nanoparticle monolayers covered with sol-gel oxide thin films: optical and morphological study, Langmuir 27 (2011) 13739-13747.

[16] L.A.G. Page, R.J. McManus, Print media products for generating high quality, water-fast images and methods for making the same, US Patent No. 6869647 B2 (2005).

[17] G. Frens, Controlled nucleation for the regulation of the particle size in monodisperse gold suspensions, Nature 241 (1973) 20-22.

[18] T.V. Thu, P.D. Thanh, K. Suekuni, N.H. Hai, D. Mott, M. Koyano, S. Maenosono, Synthesis of delafossite $CuAlO_2$ p-type semiconductor using a nanoparticle-based Cu(I) acetate-loaded boehmite precursor, Mater. Res. Bull. 46 (2011) 1819-1827.

[19] K.-S. Lee, M.A. El-Sayed, Gold and silver nanoparticles in sensing and imaging: sensitivity of plasmon response to size, shape, and metal composition, J. Phys. Chem. B 110 (2006) 19220-19225.

[20] N. Nath, A. Chilkoti, Label-free biosensing by surface plasmon resonance of nanoparticles on glass: optimization of nanoparticle size, Anal. Chem. 76 (2004) 5370-5378.

[21] H.M. Kim, S.M. Jin, S.K. Lee, M.-G. Kim, Y.-B. Shin, Detection of biomolecular binding through enhancement of localized surface plasmon resonance (LSPR) by gold nanoparticles, Sensors 9 (2009) 2334-2344.

[22] K.S. Johnston, S.S. Yee, Calibration of surface plasmon resonance refractometers using locally weighted parametric regression, Anal. Chem. 69 (1997) 1844-1851.

[23] N. Matsunaga, G. Sakai, K. Shimanoe, N. Yamazoe, Diffusion equation-based study of thin film semiconductor gas sensor – response transient, Sens. Actuators B 83 (2002) 216-221.

[24] Y. Sun, Y. Xia, Increased sensitivity of surface plasmon resonance of gold nanoshells compared to that of gold solid colloids in response to environmental changes, Anal. Chem. 74 (2002) 5297-5305.

[25] L.J. Criscenti, R.T. Cygan, A.S. Kooser, H.K. Moffat, Water and halide adsorption to corrosion surfaces: molecular simulations of atmospheric interactions with aluminum oxyhydroxide and gold, Chem. Mater. 20 (2008) 4682-4693.

Biographies

Priyank Mohan obtained a BSc in Chemistry from the University of Delhi (UD), India. Currently, he is a masters student of the JAIST-UD dual education program at JAIST and working under the supervision of Prof. Maenosono.

Ryuzo Shinta obtained both a BSc and MSc in Chemistry from the Kyusyu Institute of Technology, Japan. He works as a researcher in the group of Dr. Matsumura at Nippon Steel Chemical Co., Ltd. His research interests include plasmonics, nanostructured materials, and humidity sensing technology.

Jun Fujihara received a BEng in Engineering from the Shizuoka University in 2011. He is currently pursuing the master degree in engineering at the Tokyo University of Agriculture and Technology, where he is studying gold nanostructures for moisture permeability in transparent encapsulant.

Hiroaki Takahashi obtained an MSc in Materials Science from JAIST, Japan in 2009. Currently, he is a PhD student of JAIST and working in Prof. Mizutani's laboratory. His research in JAIST has focused on second harmonic spectroscopy of TiO_2 surfaces.

Derrick Mott obtained a BSc in Chemistry from the Rochester Institute of Technology and his PhD in Materials Chemistry from the State University of New York at Binghamton in the United States. He currently is working as an Assistant Professor at JAIST, Japan under Dr. Shinya Maenosono. Dr. Motts research focuses on the fundamental design and synthesis of plasmonic nanoparticle probes and new nanoparticle based thermoelectric materials.

Yasufumi Matsumura obtained a BSc in Pharmacy from the Tokyo University of Pharmacy and Life Science, an MSc in Environmental Science from the University of Shizuoka, and a PhD in Chemistry

from the Konan University in Japan. He leads his research group at Nippon Steel Chemical Co., Ltd. His research interests include plasmonics, nanostructured materials, and sensing materials.

Goro Mizutani obtained his BSc, MSc and PhD in Physics from the University of Tokyo, Japan. He leads his research group at JAIST. His research interest is developing optical second harmonic/sum frequency spectroscopy and microscopy for analyzing surface and interface phenomena.

Kentaro Iwami received the bachelor, master, and PhD degree in engineering from Tohoku University in 2003, 2005 and 2008, respectively. He is now an Associate Professor of Tokyo University of Agriculture and Technology. His interests are in MEMS, Near-filed optics, Nanophotonics, Plasmonics, etc. Dr. Iwami received the Tohoku University President Award, Outstanding Paper Award of Workshop of E filed of IEE and AP-NFO Award in 2005, 2004 and 2003, respectively.

Norihiro Umeda received the bachelor degree and master degree in engineering from Shizuoka University in 1975 and 1977, respectively, and he received PhD degree in engineering from Tokyo Institute of Technology in 1981. He became Professor at Tokyo University of Agriculture and Technology in 1996. Current research interests are focused on Near-field optics, Plasmonics, micro/nano device, etc. Dr. Umeda received the Takayanagi Memorial Award in 2009.

Shinya Maenosono obtained his BEng and PhD from the University of Tokyo, Japan. He leads a dedicated research group in the school of materials science JAIST. His research in JAIST has focused on two main areas of interest in the field of materials chemistry and nanotechnology. The first area involves wet chemical synthesis of semiconductor nanoparticles with controlled size, shape and composition for energy conversion device applications. The second area has focused on the synthesis and bioapplication development of monometallic and alloyed multimetallic nanoparticles.

Figure captions

Fig. 1. Schematic illustration of the humidity sensing experiment setup.

Fig. 2. Schematic illustration of the experimental setup for investigating the adsorption and desorption kinetics of hexane. (a) Gas generator, (b) sample chamber, and (c) optics system.

Fig. 3. TEM images of Au NPs of D = (a) 13.5 nm, (b) 24.1 nm, (c) 48.5 nm, and (d) 78.9 nm, and (e) γ-AlOOH NRs. The inset of (e) shows the XRD pattern of γ-AlOOH NRs with the corresponding reference pattern (JCPDS card no. 01-072-0359).

Fig. 4. UV-Vis spectra of aqueous dispersions of Au NPs. From left to right, D = 13.5, 24.1, 48.5, 55.9, 67.1, and 78.9 nm. The inset shows the LSPR peak wavelengths plotted versus D.

Fig. 5. (a) Photographs of AuNPs/γ-AlOOH composite film before (top) and after (bottom) putting a water drop on the film. (b) UV-Vis spectra of the film before (red, bottom) and after (blue, top) moistening. SEM image of the surface (c) and cross-sectional TEM image (d) of the AuNPs/γ-AlOOH composite film.

Fig. 6. (a) The LSPR peak wavelength plotted versus the refractive index of the surrounding medium for AuNPs/γ-AlOOH composite films containing Au NPs of different D. From bottom to top, D = 13.5, 24.1, 48.5, 55.9, 67.1, and 78.9 nm. (b) The sensitivity factor, S, plotted as a function of D.

Fig. 7. (a) Evolution of the change in absorbance at 570 nm (ΔA_{570}) as a function of water vapor concentration (V). Solid line represents a sigmoidal fit of the data (R^2 = 0.987). The inset shows the linear scale plot of ΔA_{570} versus V. (b) Time evolutions of V measured by the AuNPs/γ-AlOOH composite film

(red curve) and a chilled mirror hygrometer (black curve) for different humidity level of moist air. The humidity level increases in a stepwise fashion at five-minute intervals.

Fig. 8. Time evolutions of the transmission intensity of the AuNPs/γ-AlOOH composite films with different *D* at fixed wavelength. From bottom to top, *D* = 13.5, 48.5 and 78.9 nm. The detection wavelengths are 520, 540 and 580 nm for *D* = 13.5, 48.5 and 78.9 nm, respectively.

Fig1

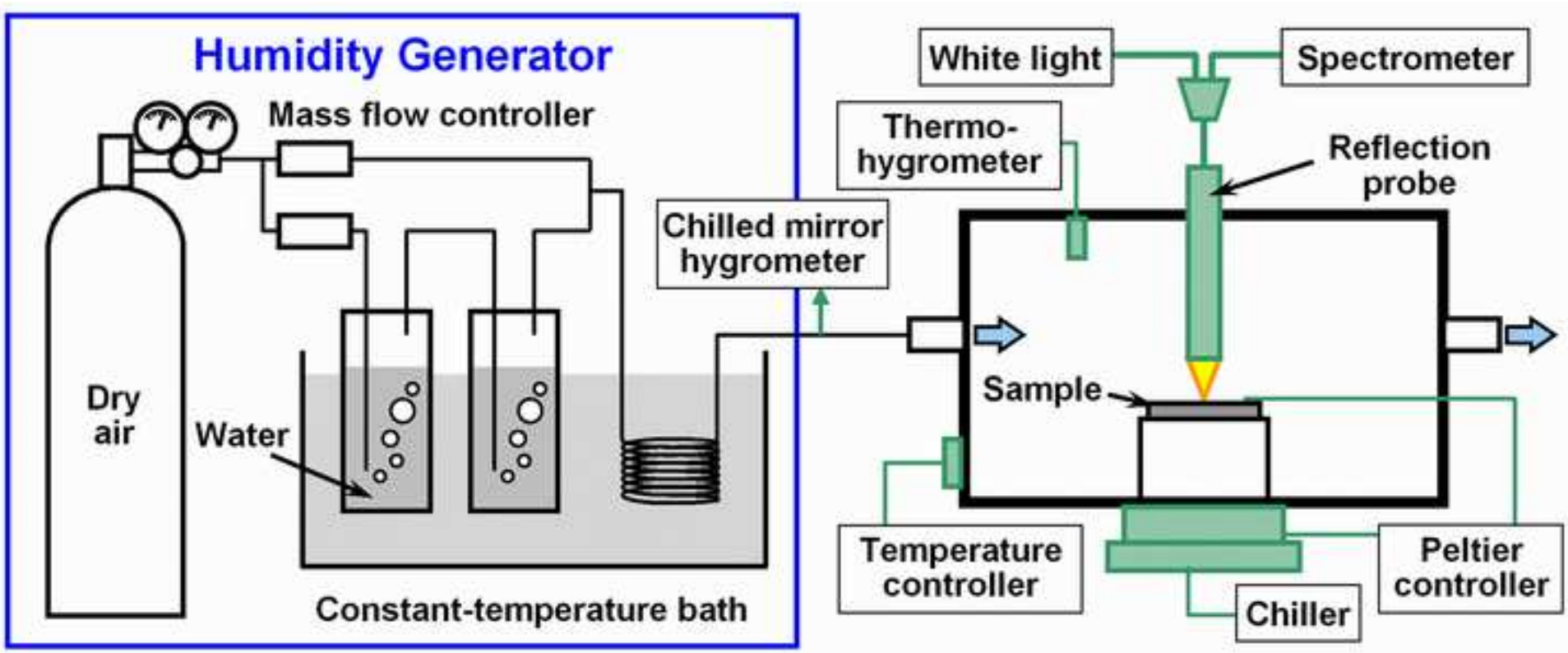
Humidity Generator
Mass flow controller
Dry air
Water
Constant-temperature bath
Chilled mirror hygrometer
White light
Spectrometer
Thermo-hygrometer
Reflection probe
Sample
Temperature controller
Peltier controller
Chiller

Fig2

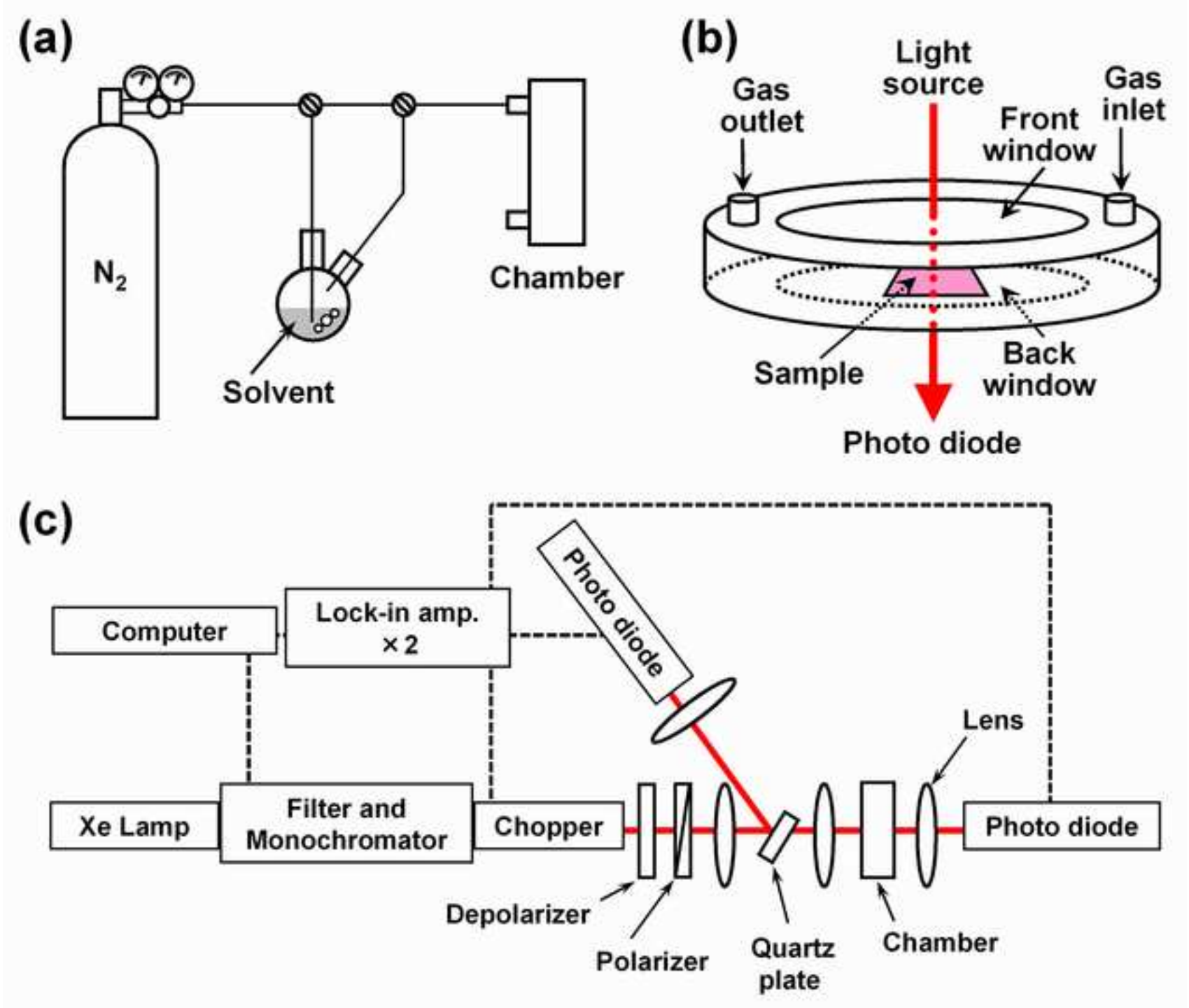
(a)
N_2
Solvent
Chamber
(b)
Gas outlet
Light source
Front window
Gas inlet
Sample
Back window
Photo diode
(c)
Computer
Lock-in amp. ×2
Photo diode
Lens
Xe Lamp
Filter and Monochromator
Chopper
Photo diode
Depolarizer
Polarizer
Quartz plate
Chamber

Fig3

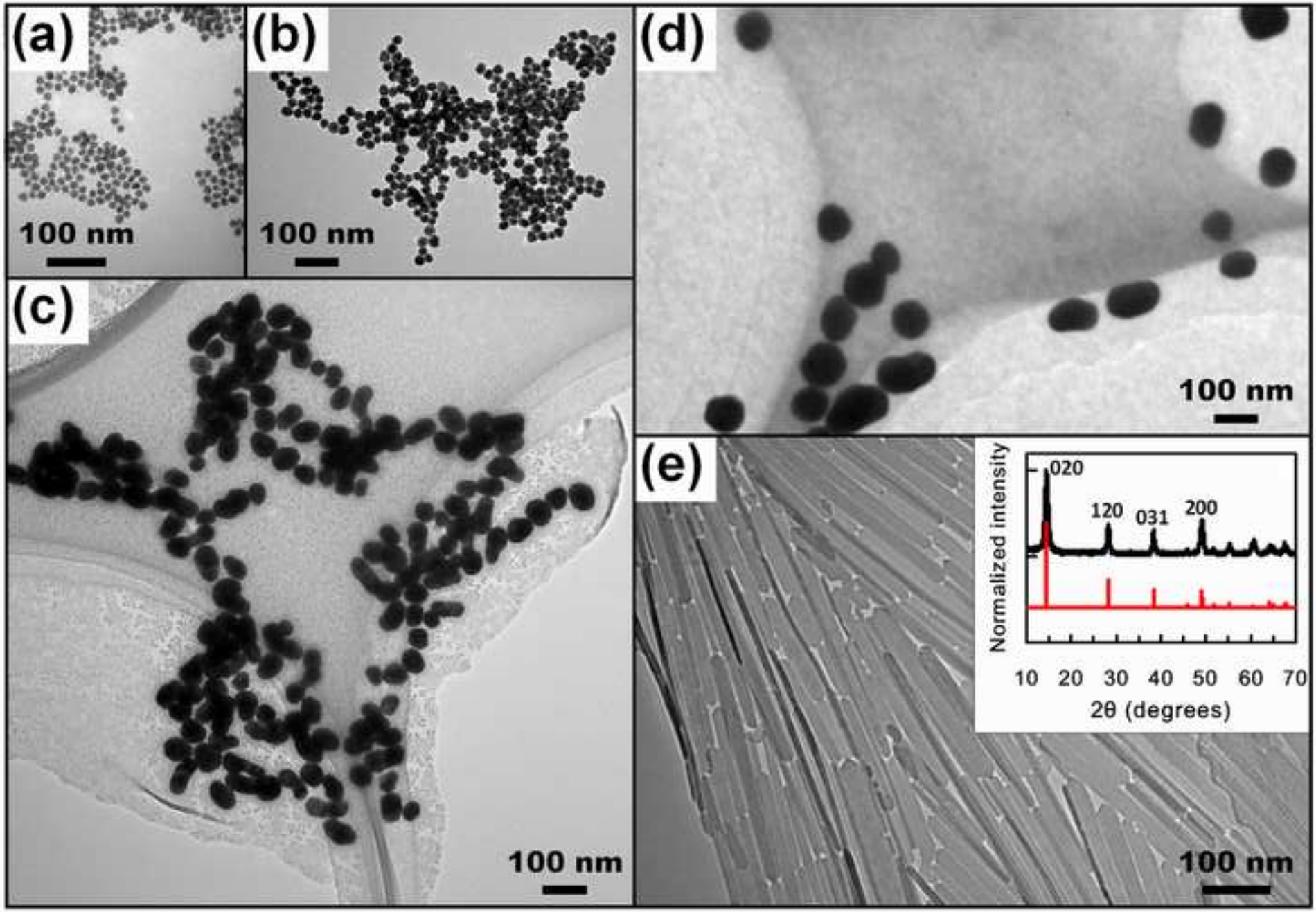
(a)
100 nm
(b)
100 nm
(c)
100 nm
(d)
100 nm
(e)
100 nm
Normalized intensity
020
120
031
200
10 20 30 40 50 60 70
2θ (degrees)

Fig4

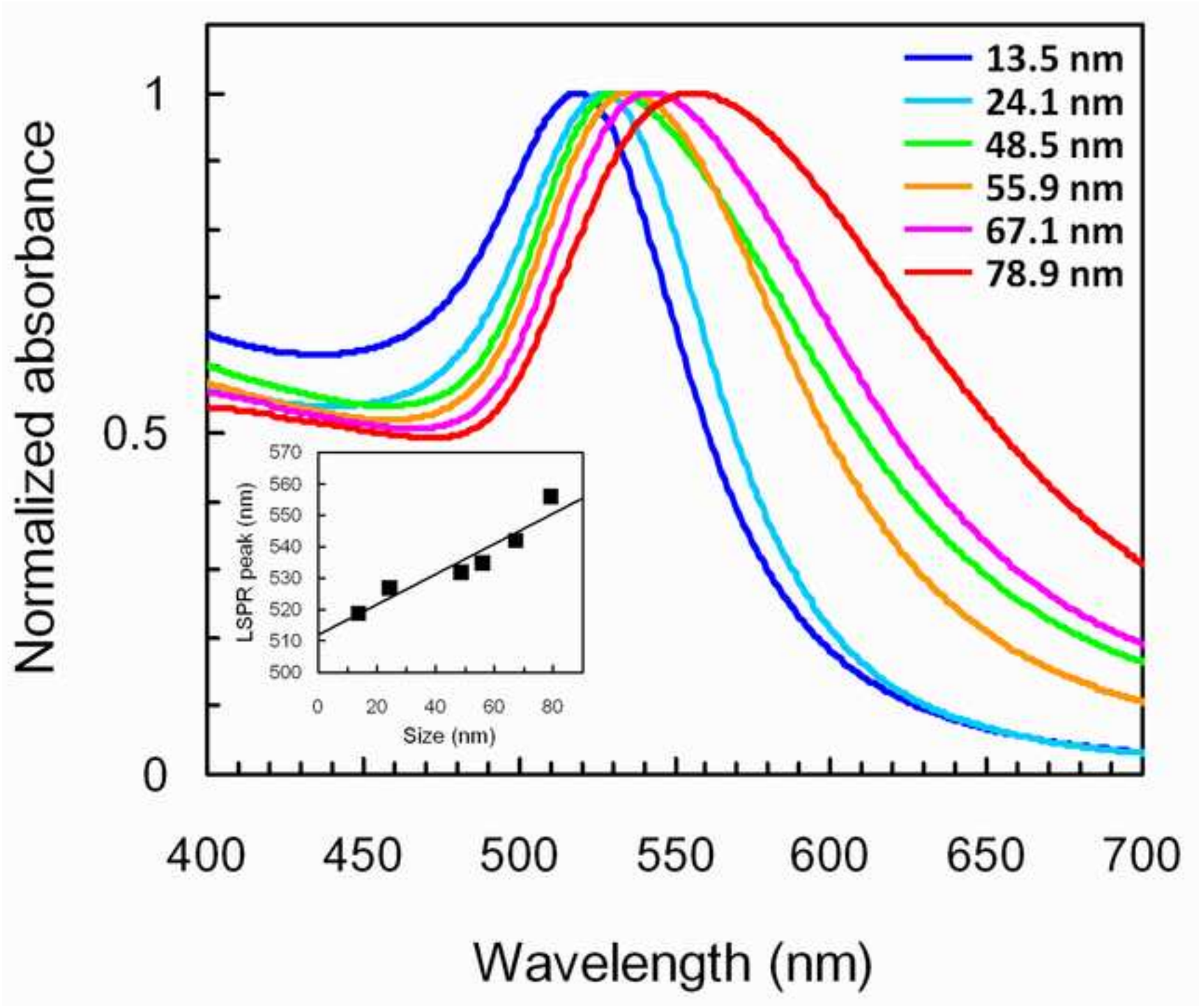
13.5 nm
24.1 nm
48.5 nm
55.9 nm
67.1 nm
78.9 nm
Normalized absorbance
1
0.5
0
400
450
500
550
600
650
700
Wavelength (nm)
LSPR peak (nm)
570
560
550
540
530
520
510
500
0
20
40
60
80
Size (nm)

Fig5

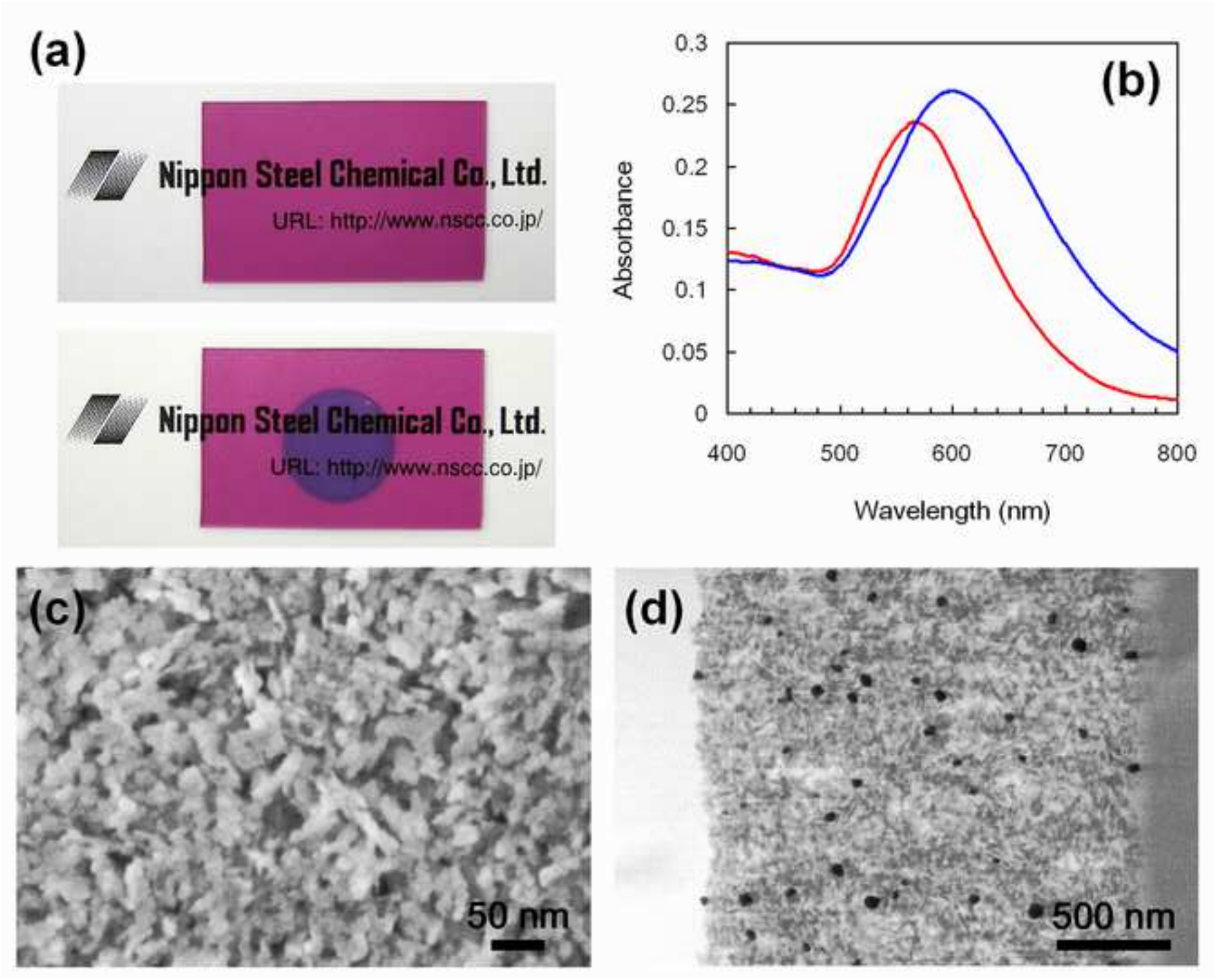
(a)
Nippon Steel Chemical Co., Ltd.
URL: http://www.nscc.co.jp/
Nippon Steel Chemical Co., Ltd.
URL: http://www.nscc.co.jp/
(b)
Absorbance
0.3
0.25
0.2
0.15
0.1
0.05
0
400
500
600
700
800
Wavelength (nm)
(c)
50 nm
(d)
500 nm

Fig6

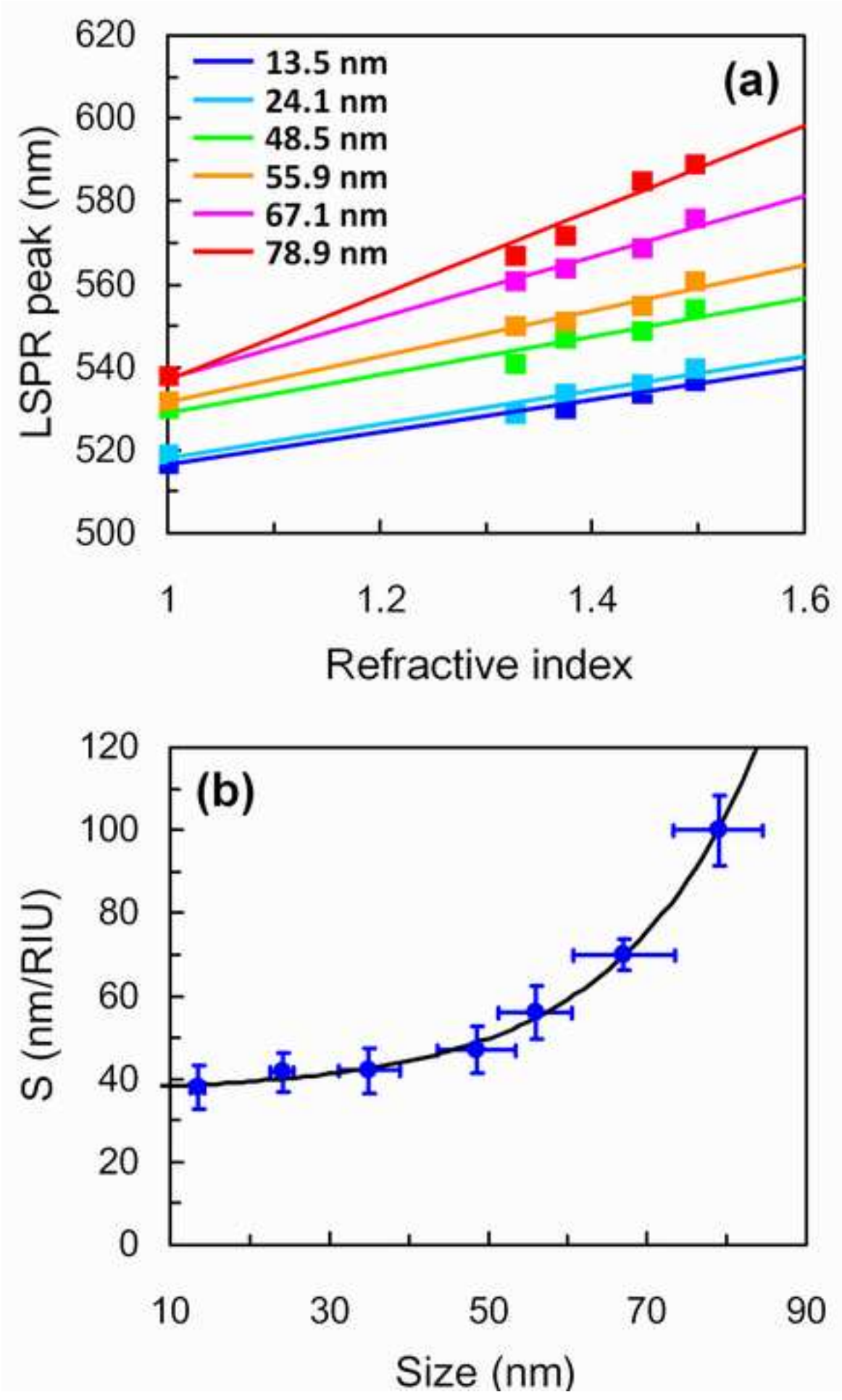
(a)
13.5 nm
24.1 nm
48.5 nm
55.9 nm
67.1 nm
78.9 nm
LSPR peak (nm)
620
600
580
560
540
520
500
1
1.2
1.4
1.6
Refractive index
(b)
S (nm/RIU)
120
100
80
60
40
20
0
10
30
50
70
90
Size (nm)

Fig7

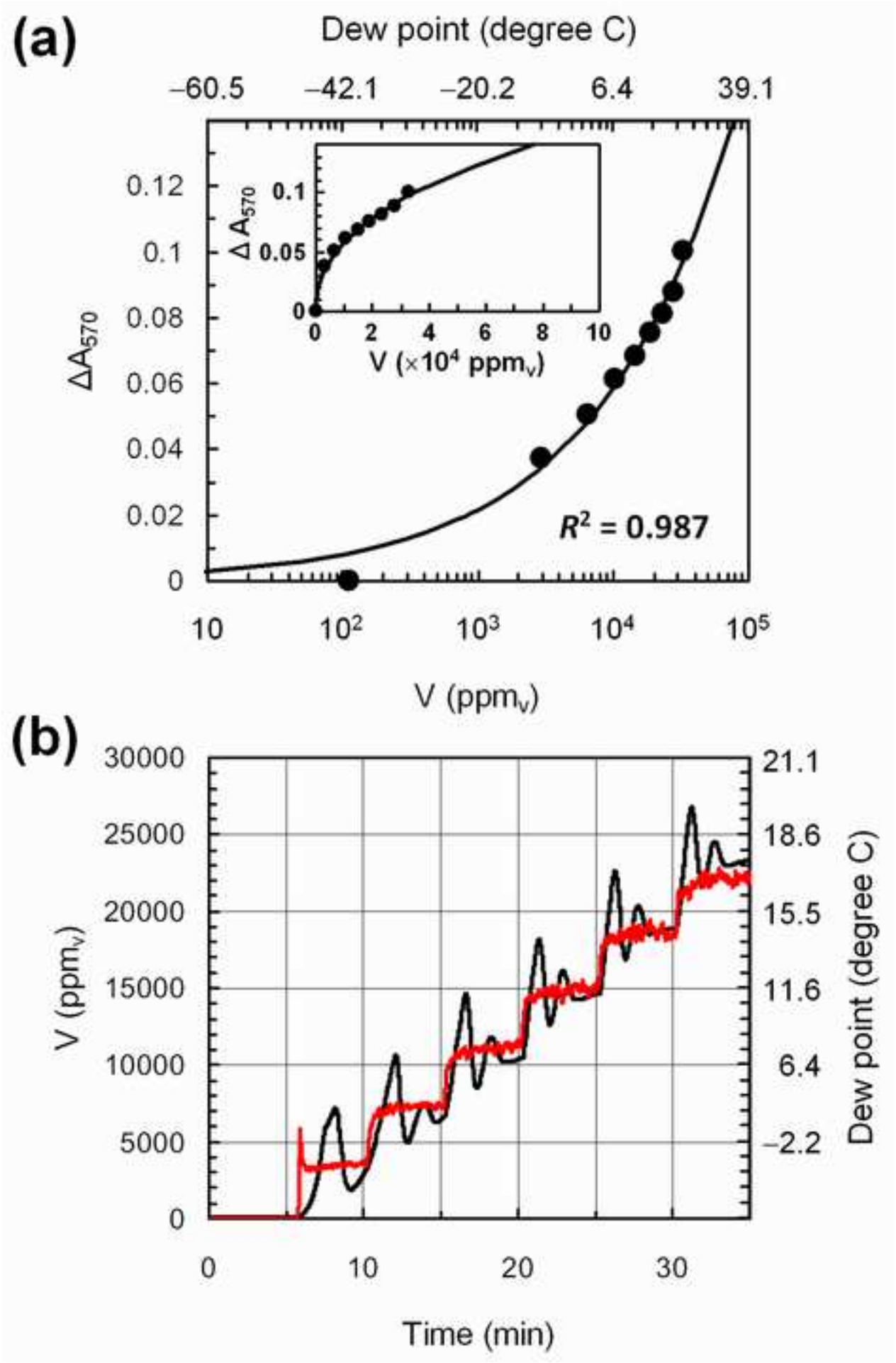
(a)
Dew point (degree C)
−60.5
−42.1
−20.2
6.4
39.1
ΔA570
0.12
0.1
0.08
0.06
0.04
0.02
0
ΔA570
0.1
0.05
0
0
2
4
6
8
10
V (×10⁴ ppmv)
R² = 0.987
10
10²
10³
10⁴
10⁵
V (ppmv)
(b)
30000
25000
20000
15000
10000
5000
0
V (ppmv)
21.1
18.6
15.5
11.6
6.4
−2.2
Dew point (degree C)
0
10
20
30
Time (min)

Fig8

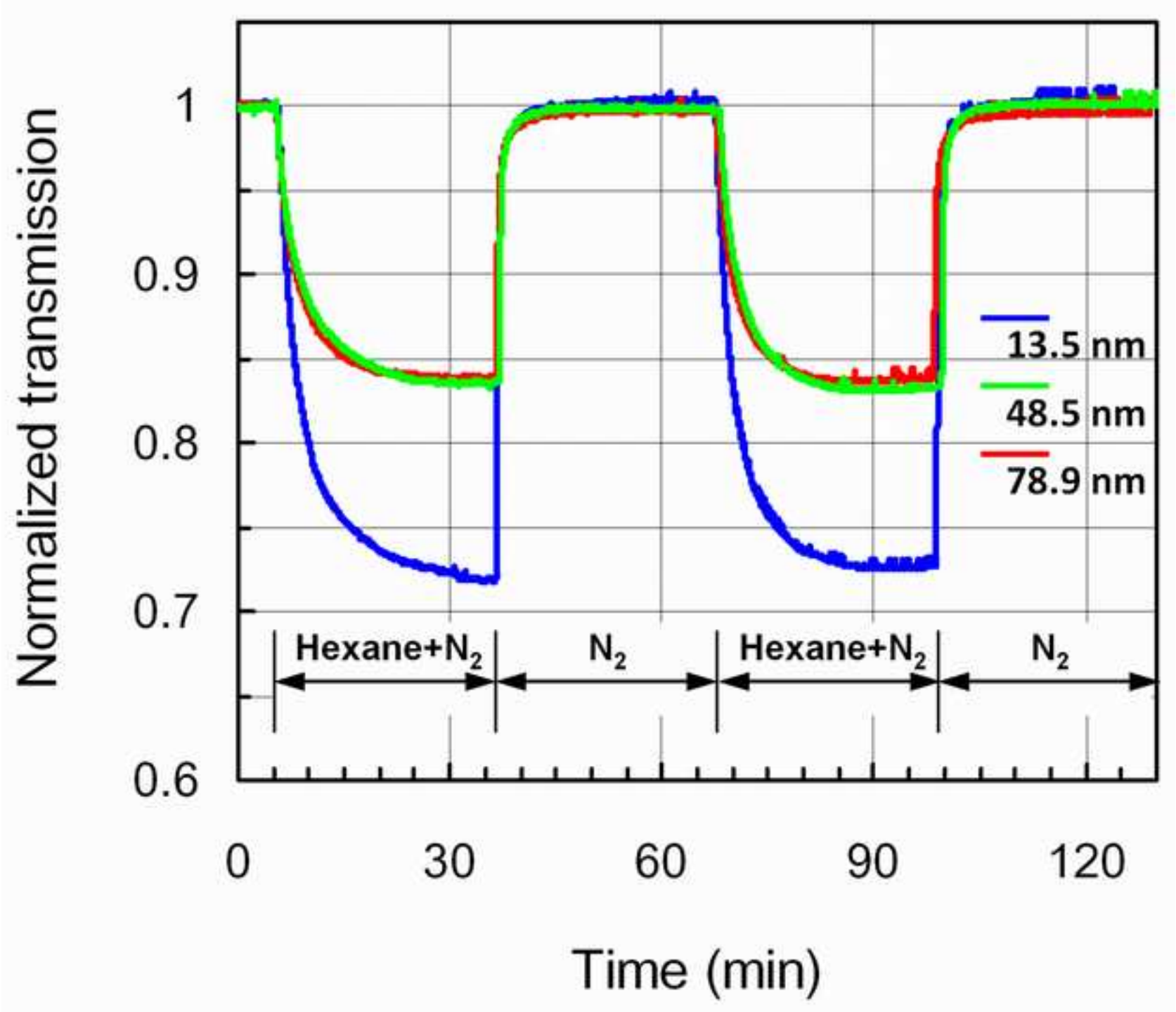
Normalized transmission
1
0.9
0.8
0.7
0.6
0
30
60
90
120
Time (min)
13.5 nm
48.5 nm
78.9 nm
Hexane+N2
N2
Hexane+N2
N2